Study of Geoelectrical Responses to Space Weather Anomalies: Auroral Latitudes, Yenisei-Khatanga Regional Trough

E. Yu. Sokolova[a, b, *], E. E. Marshalko[c], O. V. Kozyreva[a], I. S. Kupriyanov[b], D. V. Epishkin[d], V. A. Pilipenko[a], G. E. Slinchuk[d, e], D. V. Yakovlev[d], and A. G. Yakovlev[d, e]

[a] Schmidt Institute of Physics of the Earth, Russian Academy of Sciences, Moscow, 123242 Russia
[b] All-Russian Research Institute of Oil Geology, Moscow, 105118 Russia
[c] Finnish Meteorological Institute, Helsinki, FI-00101 Finland
[d] OOO Severo-Zapad, Moscow, 117545 Russia
[e] Moscow State University, Moscow, 119991 Russia
***e-mail: sokol_l@mail.ru**

Abstract—The paper presents the results of analysis of the geoelectric (telluric) field variability during the Earth's magnetic field disturbances, caused by extreme space weather events. The area of the study is the territory of the Yenisei-Khatanga Regional Trough (YKRT) situated in the auroral zone, where geomagnetic disturbances are characterized by a high level of intensity. The economic development of the YKRT as a large oil and gas-bearing area in the Russian Arctic increases the relevance of the study of possible negative impacts of space weather on future infrastructure facilities. The most serious threat to conductive industrial structures in the polar region will be posed by geomagnetically induced currents (GIC) driven by geoelectrical responses to rapid geomagnetic field changes. The analysis of the variability of telluric fields and calculations of their extreme values in the YKRT area were made using a unique magnetotelluric impedance tensor database collected by Nord West Ltd. as a result of the regional phase of the geophysical study of the trough and adjacent areas. The geoelectric field spatial-frequency distributions on the Earth's surface were calculated on the basis of the impedance estimates and harmonic approximations of the external geomagnetic excitation. The obtained maps were correlated with geological data to find areas characterized by maximal distortions of the telluric field. Extreme amplitudes of geoelectrical responses at a series of representative locations in the YKRT were evaluated on the time series of telluric field variations, synthesized through the impedance dependences on frequency and magnetic field time series recorded during geomagnetic storms and substorms at the nearest stationary monitoring sites. The resulting estimates of amplitudes and directions of geoelectric fields during space weather disturbances can be used to account for possible destructive effects of GIC in design of pipelines, power transmission lines and railways.

INTRODUCTION

The theoretical and practical value of studying the Earth surface manifestations of space weather events significantly increased in the 21st century that was marked by the accelerated economic development of high-latitude regions of Eurasia and North America (Pirjola et al., 2005; Afanasenkov et al., 2018). Russian polar regions offer experimental opportunities for such studies: a network of stationary magnetic observatories is being restored (Gvishiani and Lukyanova, 2015; Kozyreva et al., 2022) (Fig. 1), large-scale areal surveys of magnetotelluric (MT) fields are being carried out in the frames of oil and gas exploration (Afanasenkov and Yakovlev, 2018) (Fig. 2).

Monitoring of space weather determined by the dynamics of the processes in the solar, interplanetary and near-Earth plasma aims at studying the physics of solar-terrestrial relationships, interaction of planetary shells, and the influence of space factors on all spheres of life on the Earth, from biology to technology (Boteler et al., 1998; Kleymenova and Kozyreva, 2008). One of the most significant factors is geomagnetic activity that rapidly increases during magnetic storms and substorms in the auroral zone. Extreme space weather phenomena are a serious hazard to space and ground-based technological systems as sharp time-varying jumps of the geomagnetic field (dB/dt) induce electric fields in the conductive Earth (geoelectric, telluric fields), which, in their turn, generate GIC in grounded technological constructions
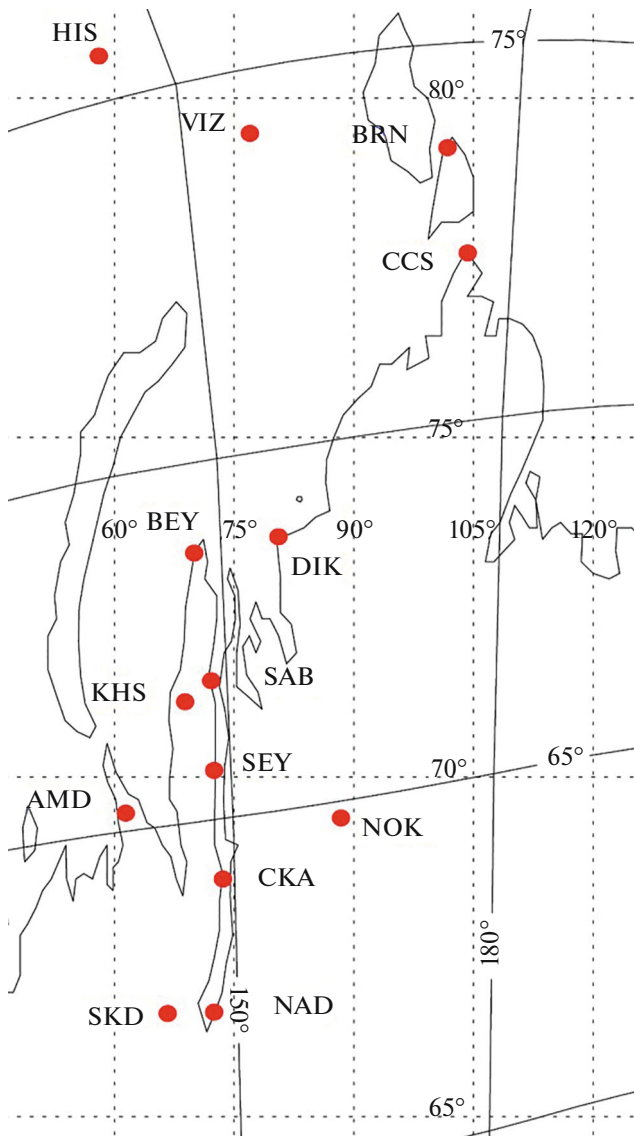
Fig. 1. Stations of geomagnetic monitoring conducted by Pushkov Institute of Terrestrial Magnetism, Ionosphere and Radio Wave Propagation (IZMIRAN), Space Research Institute (IKI), Central Arctic Research Centre of the Russian Academy of Sciences. Dotted lines indicate the geographic grid; solid lines indicate the geomagnetic grid. VIZ—Vize Island; HIS—Heiss Island; BRN—Baranov; CCS—Cape Chelyuskin; DIK—Dickson; BEY—Bely; SAB—Sabetta; SEY—Seyakha; CKA—Cape Kamenny; AMD—Amderma; KHS—Kharasavey; NOK—Norilsk; NAD—Nadym; SKD—Salekhard.

(Cannon et al., 2013; Dimmock et al., 2020; Pilipenko, 2021). The most significant threats are posed to long-distance electrical transmission lines (ETL), where GIC can produce intense jumps of quasi-stationary currents that damage high-voltage transformers (Vakhnina, 2012; Pulkkinen et al., 2017). Such phenomena are actively studied at ETL Nord Transit in Karelia and the Kola Peninsula, with the help of Russia's only system of GIC measurements (Sakharov et al., 2021; Kozyreva et al., 2019; Sokolova et al., 2019).

In the central sector of the Russian Arctic, of top priority are GIC problems in the oil infrastructure. Responses of pipelines to geomagnetic perturbations have been under investigation for quite a long time (Campbell, 1978; Brasse and Junge, 1984; Osella et al., 1998). It has been established that while GIC is flowing, the fluctuations in the pipe-to-soil potential can go beyond the set cathodic protection limits and that the cumulative effect even of small over-limits can lead to a significant acceleration of electric corrosion and reduction of the pipeline failure-free operating period. Excess potentials and GIC in grounded technological systems can be estimated on the basis of characteristics of external magnetic disturbance and induced geoelectric fields, using technical parameters of industrial structures (Pulkkinen et al., 2001; Trichtchenko and Boteler, 2002; Morales et al., 2020).

Assessment of risks associated with space weather is a multifaceted science and technology issue that is becoming more and more important with the advancement of technologies and the increasing dependence of the Earth's civilization on them. Understanding the causes of the origin and patterns of GIC sources is the domain of geophysical research. Strong GIC in high latitudes are produced not only by large-scale auroral electrojets but also by relatively weak and minor, yet rapid processes (Belakhovsky et al., 2018; Kozyreva et al., 2020; Apatenkov et al., 2020; Chinkin et al., 2021; Dimmock et al., 2019). Among the main GIC sources are: explosive auroral substorm commencements, irregular Pi3/Ps6 pulsations with steep edges and complex topology of dB/dt variability, long-lasting quasi-monochromatic Pc5 pulsations that can have a cumulative destructive effect both on transformers and on pipelines (Pilipenko, 2021).

In fact, GIC originate not from the variability of the geomagnetic field dB/dt as such but from telluric fields determined by the geoelectric structure of the region of the study. Understanding the nature of GIC and how realistic are GIC predictions is inextricably linked with how well we understand depth distribution of electrical conductivity (Bedrosian and Love, 2015; Sokolova et al., 2019; Kelbert, 2020). The necessary information on the geoelectric structure can be obtained from MT sounding data. To measure possible GIC across the USA, the data collected during large EarthScope MT sounding of were used (Bedrosian and Love, 2015; Love et al., 2016; Lukas et al., 2018). A consolidated array of MT sounding data from Canadian provinces Alberta and British Columbia formed the backbone of the estimates of telluric fields during periods of intense geomagnetic events (Cordell et al., 2021). This paper demonstrates advantages of using experimental MT impedance estimates reflecting realistic three-dimensional (3D) distribution of electrical conductivity over model approximations of limited dimensions, much used in studying geomagnetically induced fields. Another recent trend is the use of real-data-based regional or global 3D electrical con-
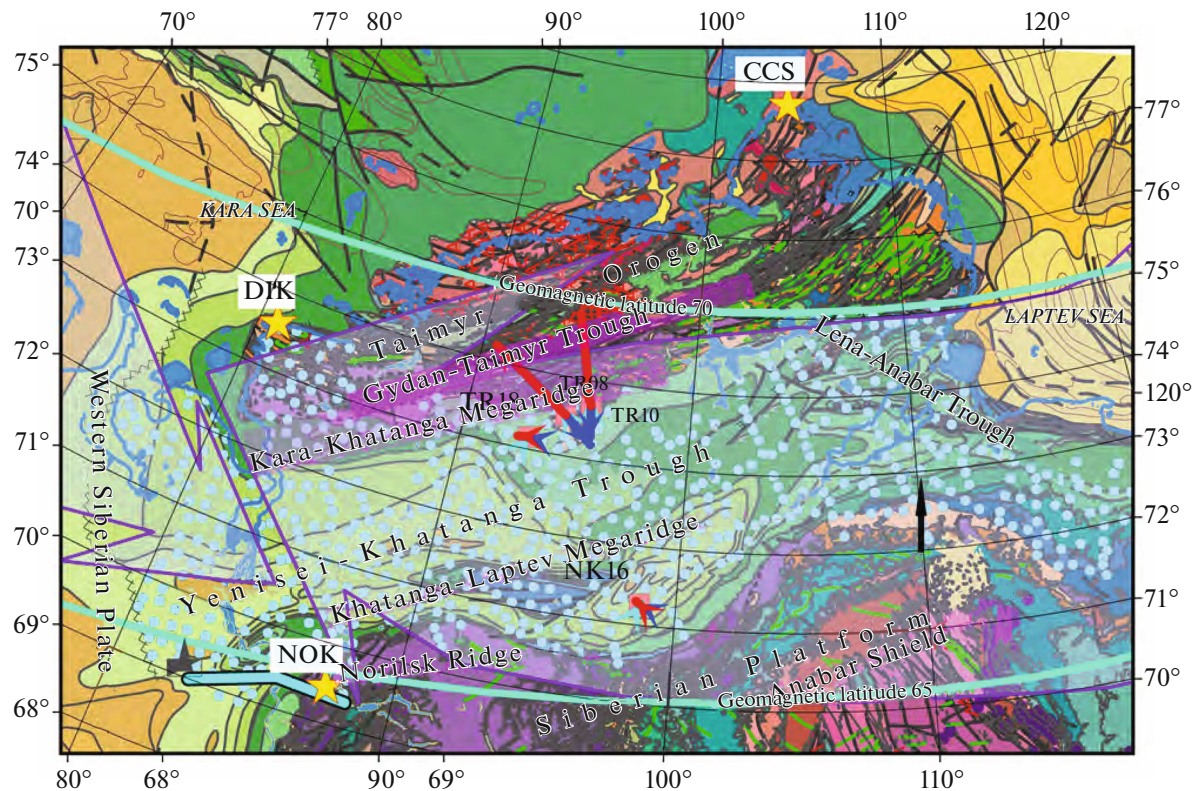
Fig. 2. Yenisei-Khatanga Regional Trough MT sounding locations (Slinchuk et al., 2022) (blue dots) and the nearest magnetic stations (DIK, CCS, NOK, yellow stars) on the background of the region's geological map, with main tectonic classification elements. For locations NK16, TR18, TR08, TR10, the figure shows vectors of a geomagnetically induced electric field, synthesized by corresponding complex impedance estimates and the 24 hour-long variation of the magnetic field at DIK during a geomagnetic storm on May 10–13, 2019 (Fig. 5): blue arrows—at 20 hours 8 minutes, pink arrows—at 22 hours 43 minutes (the black arrow—1 V/km scale vector). Blue sections show the location of the Messoyakha-Norilsk gas pipeline, transparent purple arrows show a schematic position of sub-storm ionospheric currents (western and eastern electrojets) at local midnight on the 100th meridian east.

ductivity models (Püthe and Kuvshinov, 2013; Dimmock et al., 2019; 2020; Marshalko et al., 2021; Kozyreva et al., 2022).

Most recent studies use a plane wave approximation of external magnetic excitation, which generally provides quite an adequate insight into the characteristics of geoelectrical responses (Dimmock et al., 2019; Marshalko et al., 2021). Yet, more accurate and detailed estimates of GIC drivers require considering spatial external field heterogeneity. To do this, it is necessary to have, in the first place, dense networks of magnetic stations (Pilipenko et al., 1998). Approaches to creating and using heterogeneous source models are found in research papers (Püthe and Kuvshinov, 2013; Ivannikova et al., 2018; Marshalko et al., 2021).

This paper describes the experience of studying spatio-temporal variations of geoelectric fields in the vast area of the Yenisei-Khatanga Regional Trough (YKRT), the largest oil and gas-bearing depression in the northern margin of the Siberian platform, which is going to face growing GIC problems in the coming years. The analysis uses unique broad-band MT sounding data embracing the entire trough and areas

adjacent to its edges (Slipchuk et al., 2022), as well as data from the network of magnetic stations in the Russian Arctic (Kozyreva et al., 2022). The paper presents the array of impedance estimates used and intensive geomagnetic events selected for the analysis; then, the paper describes approaches to the estimation of the geoelectrical responses to harmonic excitation and to realistic magnetic disturbances. In the end, the results of the presented analysis are discussed in terms of possible destructive effects of GIC in relation to existing and future oil infrastructure facilities in the YKRT area, and the prospects for adjustment of the obtained estimates are analyzed.

EXPERIMENTAL DATA AND ANALYSIS METHODS

Magnetotelluric Impedances

Nowadays, profile-variant MT sounding along with 2D Common Depth Point Method (CDPM) seismic surveys are the basic techniques used in the regional geophysical studies of oil and gas-bearing areas (Afanasenkov et al., 2018). The MT dataset, used

in this study, for the Yenisei-Khatanga region and the adjacent neighbouring Gydan and Anabar-Khatanga oil and gas-bearing areas was created by Nord West Ltd, following the regional phase of their geophysical study in 2008−2020 (Afanasenkov and Yakovlev, 2018; Slinchuk et al., 2022). Electrical exploration was carried out using Canadian Phoenix-Geophysics high-performance digital MTU stations and modern remote-reference sounding techniques. In terms of the network density and coverage of high-latitude areas, the resulting array of MT data has no analogues in the world. The study used an areal collection of broad-band frequency dependences of complex-valued MT impedances $Z(f, x, y)$ for 654 points (x, y) at irregular grid nodes, with an average distance between them of ~20−70 km (Fig. 2).

The study region lies almost entirely in the auroral zone, which causes additional difficulties in estimating the MT transfer functions due to the distorting effects of heterogeneous external excitation sources, mainly, auroral electrojet fields and local ionospheric-magnetospheric current structures. However, the BEAR depth sounding (Fennoscandia) as well as recent analysis of data on the exploration sounding in the YKRT and the Lena-Anabar Trough showed that modern MT observation processing methods are effective in obtaining undistorted estimates of transfer functions (as functions of the distribution of electrical conductivity and not of the source configuration) at a reasonable correspondence of observation time and maximum estimation period (Sokolova and Varentsov, 2007; Pogrebnykh et al., 2022).

Estimates of impedance tensors $Z(f, x, y)$ in the period range from 0.003 s to 1000−1800(2000) were obtained for the YKRT region on the basis of the data of 12−24-hour (or longer-term) observations of the electromagnetic field and are characterized by an accuracy meeting the current exploration MT sounding standards: up to 5% by amplitude and 3° by phase. The main tool used to obtain the estimates was the EPI-Kit software (Epishkin, 2016). The program uses low-distorted data pre-selection procedures and an advantageous remote-reference detection scheme that significantly reduces electromagnetic noise, as well as the effects of external source inhomogeneity. The penetration depth is over 20 km within a massive sedimentary cover of the trough and over 60 km in its edges, composed of high-resistivity formations. Typical broad-band frequency dependences of $Z(T)$ components estimated for four YKRT points with various geoelectrical sections are shown in Fig. 3. Further on, they are used to demonstrate the methods and results of the study.

The interpretation of MTS data for the YKRT region—from analyzing spatial distributions of the effective apparent resistivity at various field penetration depths (Fig. 4a) to the construction of 3D electrical conductivity models (using the software (Kelbert

et al., 2014)), revealed their high resolution with respect to numerous electrical conductivity heterogeneities (Slinchuk et al., 2022). The obtained data on structural and compositional complexes with various conductive properties are used in oil and gas prospecting as well as for building YKRT deep structure and geodynamic history models (Afanasenkov and Yakovlev, 2018; Andreev et al., 2021).

Meanwhile, the high potential of this impedance collection as a unique source of data on the variability of the geoelectric field—the key parameter for measuring GIC at the region's oil infrastructure facilities - has never been studied before, which makes our effort very important.

Magnetic Data

Data on intense space weather events reflected in increased geomagnetic activity within the studied area in the central sector of the Russian Arctic were taken from digital archive records of the Soviet/Russian Arctic magnetic stations (Kozyreva et al., 2022). The archive contains three-component 1-minute magnetic records from the stations in the Arctic zone of the Russian Federation for the period from 1983 to the present day, and is available at ftp://door.gcras.ru/ftp_anonymous/ARCTICA_Rus/.

Figures 5 and 6 show examples of magnetic records of several space weather events. For a general description of the interplanetary space environment, the same figures show changes in the density of the solar wind plasma Np, the solar wind velocity V and the vertical component of the interplanetary magnetic field Bz (OMNI database https://omniweb.gsfc.nasa.gov). All considered geomagnetic events are associated with the interaction of a high-speed solar wind stream (Vmax ~ 700−800 km/s, Np ~ 30−40 cm^{-3}) with the Earth's magnetosphere, which causes moderate magnetic storms with $|Dst|$ ~ 50−60 nT. During these storms, intense substorms (~1000 nT) are observed in the Earth's night-time sector. The demonstrated events are of significance when dealing with GIC excitation problem, because they include intervals with rapid variations (see also Fig. 7, Fig. 9), the physical nature of which has not yet been fully explained.

Approaches to the Estimation of Geoelectric Fields

Geoelectrical responses were synthesized via MT impedance tensors: in the frequency domain—using harmonic approximations of the external magnetic field, in the time domain—on the basis of real time records of intense magnetic disturbances.

Following (Bedrosian and Love, 2015), the first approach (the frequency domain) uses as external excitation the simplest model of uniform in space magnetic disturbances in the form of a plane harmonic wave with a period T and an individual ampli-
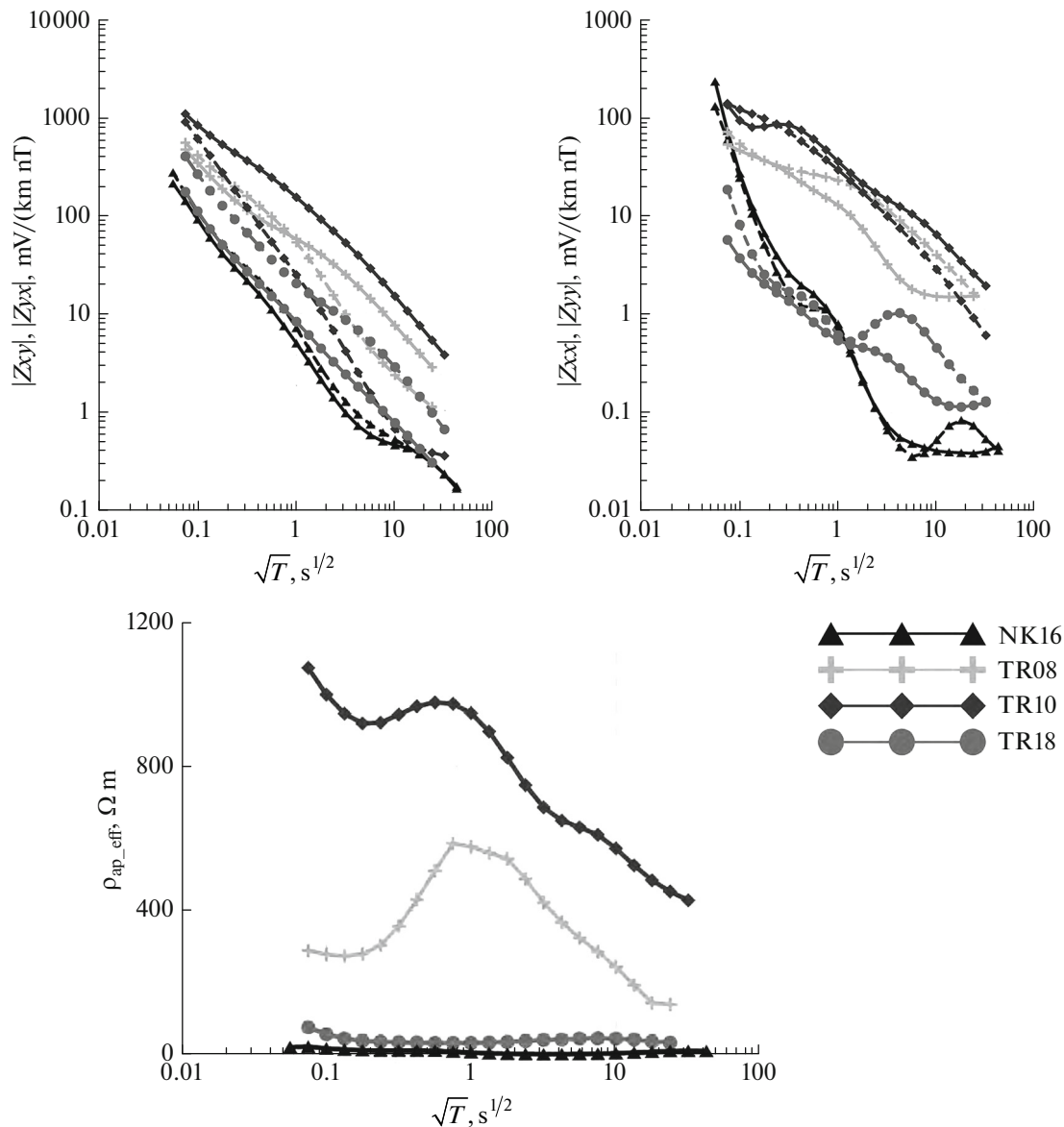
Fig. 3. Frequency dependences of amplitude components of the impedance tensor (xy/xx—solid-line curves, yx/yy—hatched curves) and effective apparent resistivity ($\rho_{ap\_eff} = 0.2Z_{eff}^2$) at the sounding locations TR10, TR08, TR18, and NK16 (Fig. 2). Axes x,y correspond to the geographic north and east directions.

tude $B_h(T) = B_h\exp(-i2\pi t/T)$, $B_h = 1$ nT oscillating in two directions: geographic N-S or E-W. Calculating horizontal electric field vectors via available MT impedances in the basic dependence $E(T, x, y) = Z(T, x, y)B_h(T)$ helps to immediately analyze spatial-frequency distortions of the incident plane wave by effects of realistic electrical conductivity heterogeneities in the Earth interiors.

The second approach is indicative of the dynamics (changes in the time domain) of the response of a realistic 3D conductivity structure to a specific temporal variation of the magnetic field, and helps to estimate

possible extreme amplitudes of the geoelectric field in the area of the study. In the absence of a synchronous array of electromagnetic observations, a dedicated program is used to synthesize the time series of the electric field $E(t, x, y)$ using given MT impedance frequency dependence $Z(f, x, y)$ and a specific time series of anomalous variations $\Delta B(t, x, y)$. The program, which is based also on a plane-wave external field model, uses the EPI-Kit MT processing environment and stable routines of forward and inverse Fourier transforms.

The algorithm of synthesis of the telluric field $E(t)$ using the geomagnetic field $\Delta B(t) = \{H(t), D(t)\}$
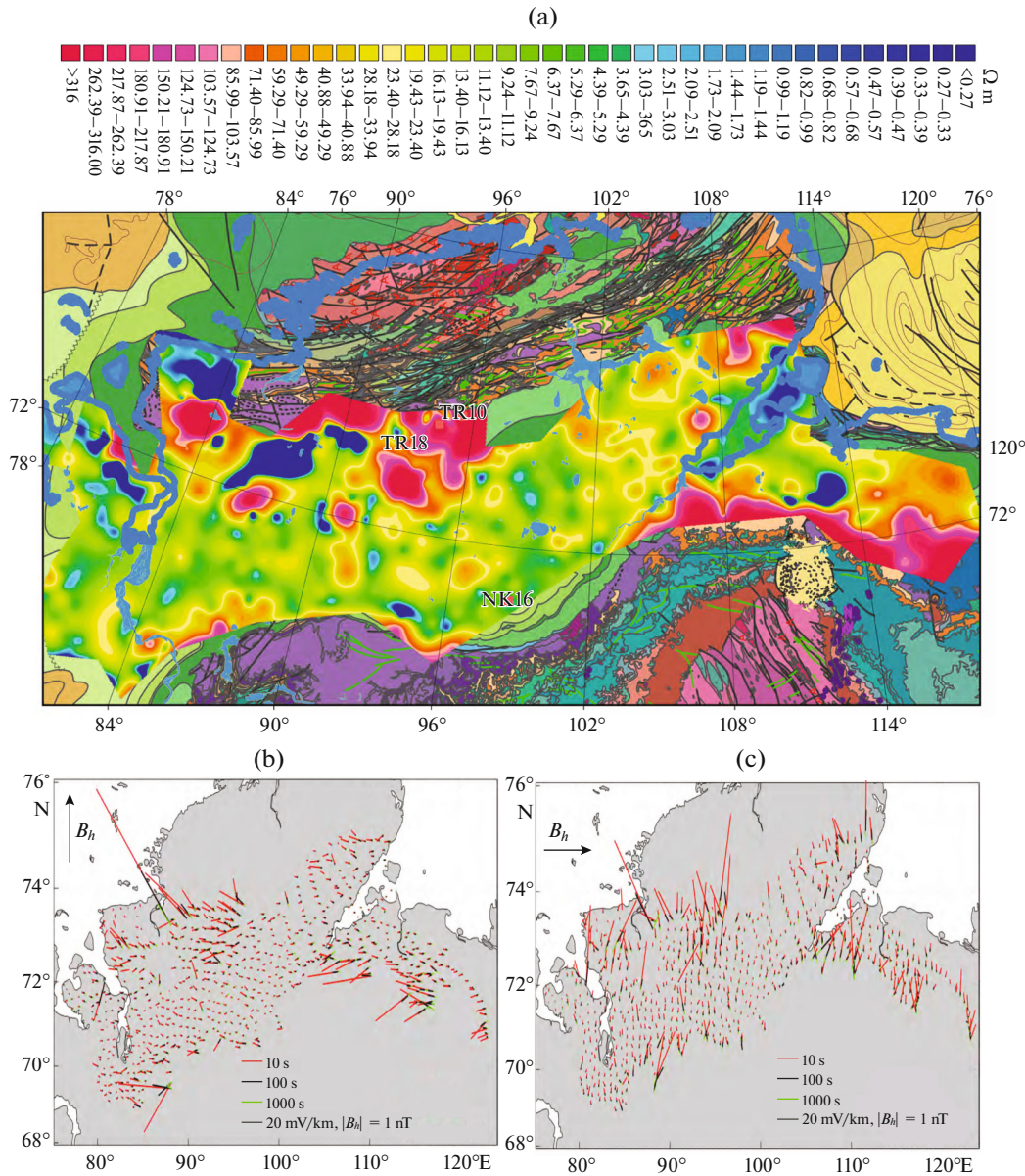
Fig. 4. Spatial distribution of effective apparent resistivity ρ_{ap_eff} over the YKRT area for $T = 10$ s according to the areal array of MT impedance estimates (Slinchuk et al., 2022) (a), and the impedance-based spatial distributions of vectors of the horizontal electric field $E(x, y, T)$, induced by the homogeneous harmonic geomagnetic field $B_h(T)$ with an amplitude of 1 nT, geographically oriented N−S (b) and E−W (c), for the periods 10 s (red), 100 s (black), and 1000 s (green); a map of electrical conductivity averaged by the upper 10 km layer in the model (Alekseev et al., 2015) (d), and amplitude geoelectrical responses, calculated in the model, to excitation by the homogeneous harmonic geomagnetic field $B_h(T)$ with a unit amplitude for the periods 10 s (e) and 100 s (f) (fragments of the maps built for the territory of the Russian Federation in (Kozyreva et al., 2022)).

(where H—is the northern component in geomagnetic coordinates, and D is the eastern one) uses the fundamental MT dependence of electric $E(f) = \{E_H(f), E_D(f)\}$ and magnetic $\Delta B(f) = \{H(f), D(f)\}$ fields in the frequency domain through the full complex impedance tensor $Z(f)$ (Berdichevsky and Dmitriev, 2009):

$$\begin{pmatrix} E_H(f) \\ E_D(f) \end{pmatrix} = \begin{pmatrix} Z_{HH} & Z_{HD} \\ Z_{DH} & Z_{DD} \end{pmatrix} \begin{pmatrix} H(f) \\ D(f) \end{pmatrix}, \quad (1)$$

where the impedance tensor components are given in practical units (mV km^{-1} nT^{-1}) and rotated to geomagnetic coordinates.

The Fourier transform is applied to overlapping sequential segments (sliding time windows Δt) of the geomagnetic field record under analysis in order to obtain a set of spectral estimators $\Delta B(f)$ and, via equations (1), corresponding telluric field estimates $E(f)$. The inverse Fourier transform is used for each time
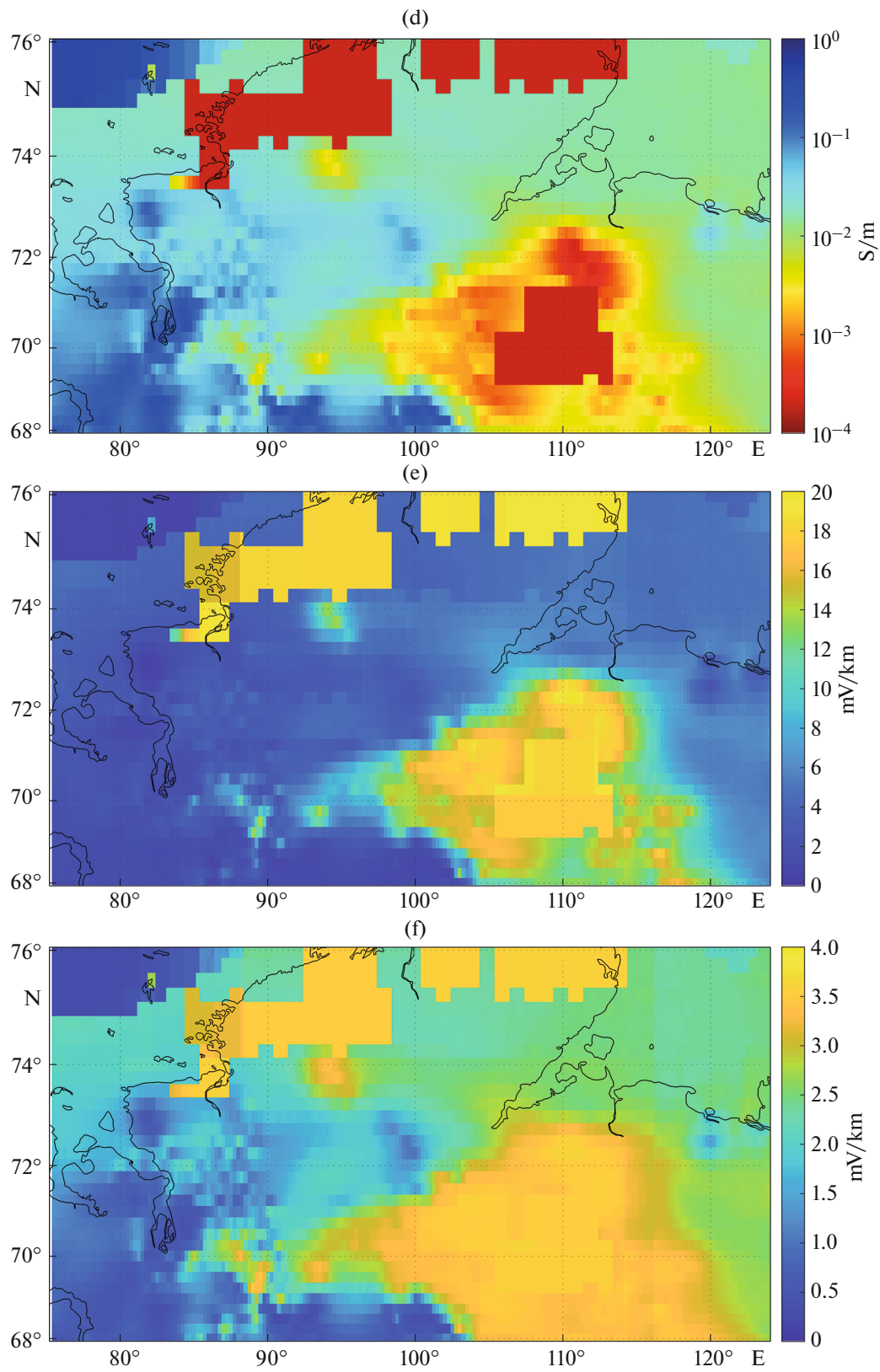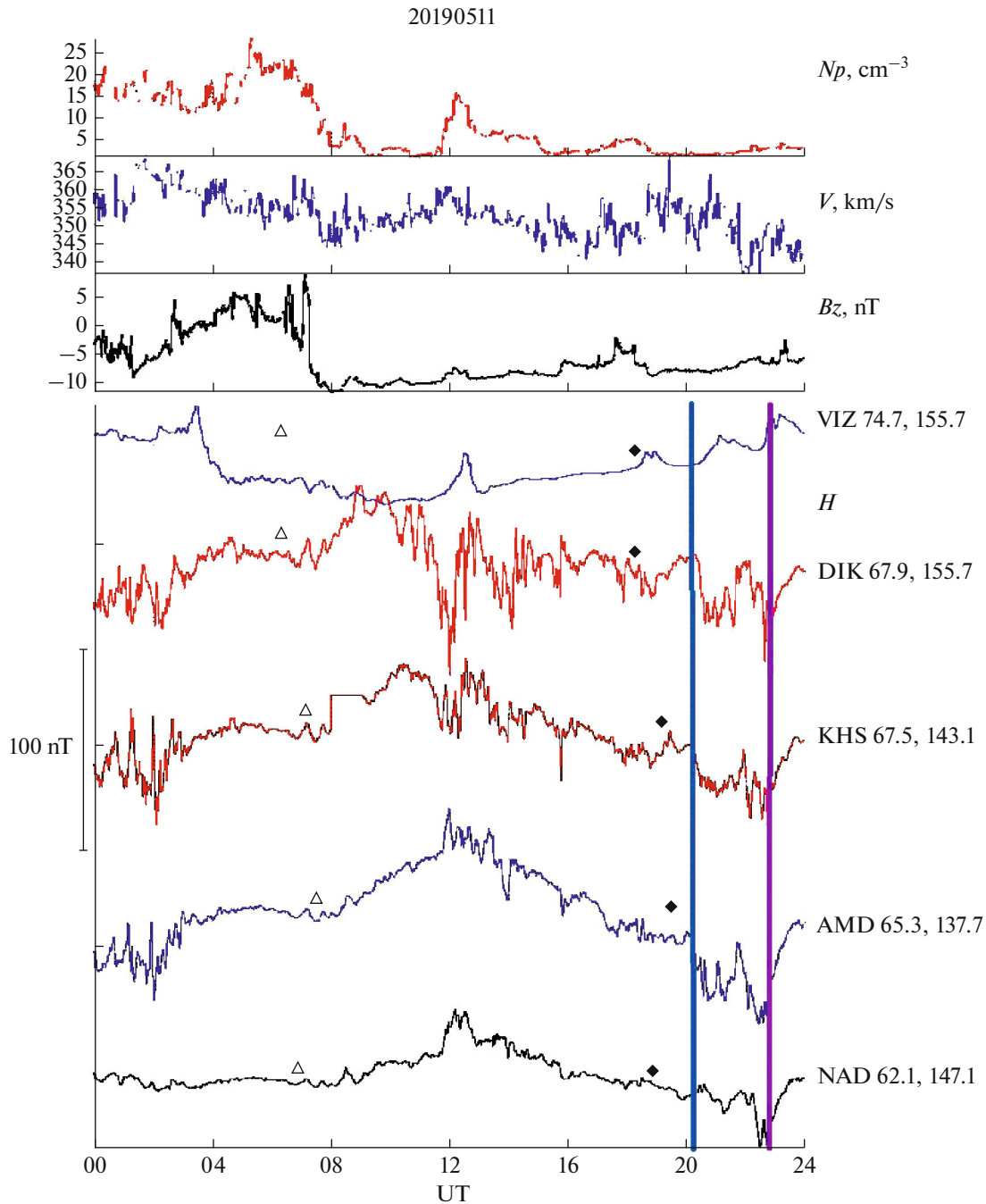
Fig. 4. (Contd.).

Fig. 5. Variations of the magnetic field H-component (towards geomagnetic north), recorded at VIZ, DIK, KHS, AMD, NAD (by $140°-150°$ magnetic longitude profile, geomagnetic coordinates of stations in degrees), in the interval 00−24 UT on May 11, 2019. Three graphs on top: variations in the density (Np), velocity (V) of the solar wind and Bz—component of the interplanetary magnetic field. Triangle symbols indicate local midday, diamond symbols stand for midnight. The blue and pink vertical lines indicate the time points 20:08 UT and 22:43 UT, accordingly, for which Fig. 2 shows vectors of synthesized geoelectrical responses at NK16, TR18, TR08, TR10.

window. In this way, until the moment corresponding to the mid-point of each of the windows, several electric field estimates are accumulated and are averaged to stabilize the calculation of the final time series of the synthetic electric field $E(t)$ corresponding to the magnetic record. The software implementation of the algorithm has successfully demonstrated its correctness on synthetic magnetic and electric time series of the COMDAT project (Ernst et al., 2003).

Telluric fields at the target points (x, y) of the Yenisei-Khatanga Trough were synthesized for several dramatic space weather events. Fragments of time series
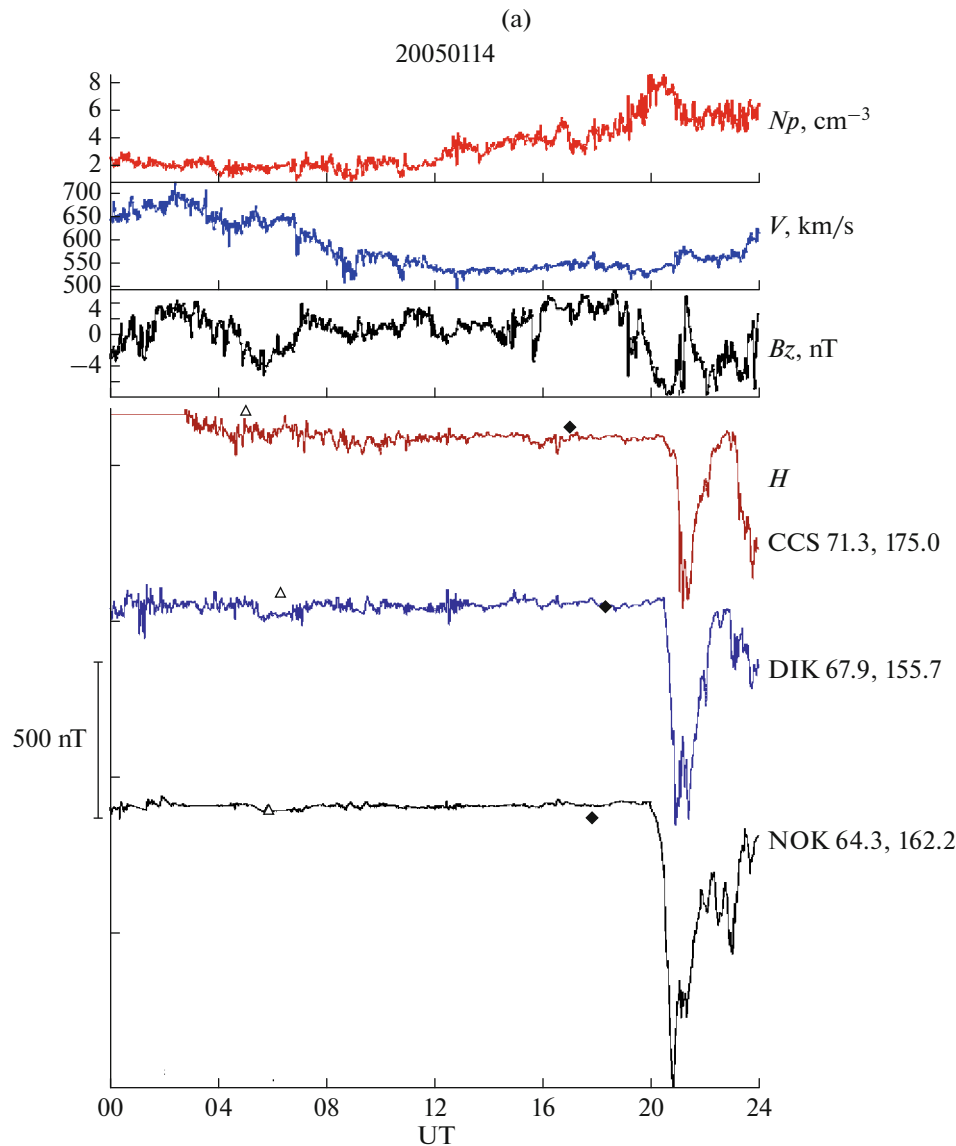
(a)

Fig. 6. Variations of the magnetic field *H*-component (towards geomagnetic north), recorded at CCS, DIK and NOK in the interval 00−24 UT on January 14, 2005 and 00−24 UT on February 8, 2005. Three graphs on top: variations in the density (*Np*), velocity (*V*) of the solar wind and *Bz*—component of the interplanetary magnetic field. Triangle symbols indicate local midday, diamond symbols stand for midnight.

of intense variations $\Delta B(t, x_0, y_0)$ at the stationary geomagnetic observation site (x_0, y_0) closest to (x, y) (from the digital 1-minute record archive (Kozyreva et al., 2022)) were used as the input signal $\Delta B(t, x, y)$.

Synthesized temporal geoelectrical responses (Fig. 7, Fig. 9), discussed below, were obtained with 1-minute discretization, on the basis of 24- and 8-hour geomagnetic observation series (Fig. 5, Fig. 6a), using a sliding 128-sample window (for the forward transform—calculating magnetic field spectra, and for the inverse Fourier transform—restoring telluric field series based on calculated spectra $E(f)$). For purposes of calculation stability, experiments with several windows were

carried out (128\256\512). To be able to work with big windows, impedance curves (maximum periods 1500−1800 s, Fig. 3) were extrapolated, as necessary, to the domain of longer periods. The results of the experiments showed minor differences in the obtained time series of geoelectrical responses.

Based on these considerations, estimates of possible extreme amplitudes of geoelectric field variations in the YKRT region based on the results of the synthesis of geoelectric fields can be regarded as sufficiently reliable, at least in the period range of 120−1000−1250 s, which is important from the perspective of GIC studies.
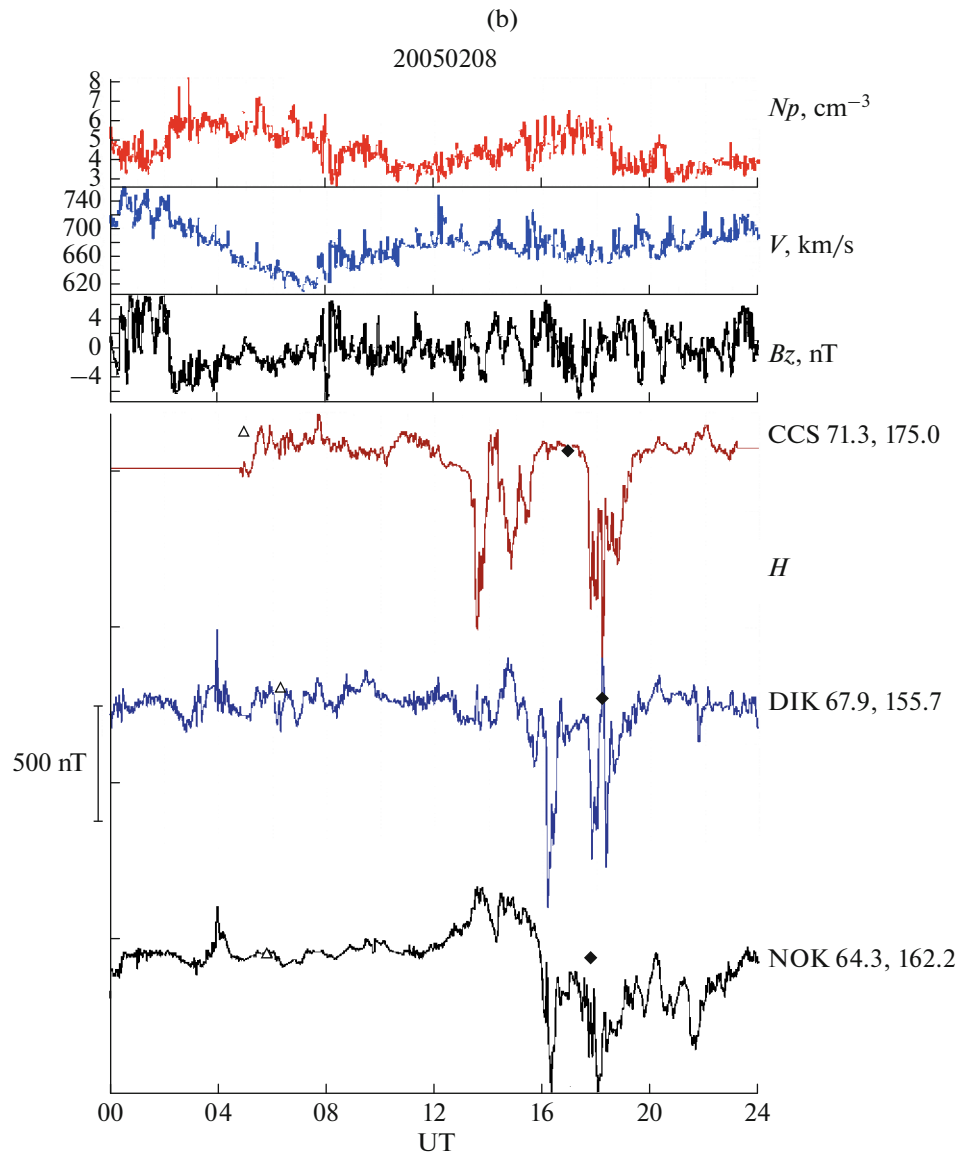
Fig. 6. (Contd.).

DISCUSSION

The Yenisei-Khatanga Regional Trough, stretching East-West for over 1000 km, is filled with a layer of nearly 20 km of Mesozoic (MZ), highly-conductive sediments with electrical resistivity of $\rho = 5{-}20$ Ω m (Afanasenkov and Yakovlev, 2018) (Fig. 2). Its edges border the Siberian Platform (the Norilsk Ridge and the Anabar monoclinal scope) in the south and the Taimyr orogen in the north, which are composed of consolidated Paleozoic and older sedimentary and metamorphic complexes ($\rho \geq 100{-}400$ Ω m). They are partially overlain by trap formations, penetrated by even more resistive intrusive formations and broken by faults. Numerous basement uplifts were geophysically established within the trough bed: the Kara-Khatanga and Khatanga-Laptev Ridges, the Yangodo-Gor-

bitsky Uplift (YGU), and others. Spatial distributions over the YKRT area of effective apparent resistivity $\rho_{ap\_eff}(T) = 0.2 Z_{eff}^2(T)$, $Z_{eff} = |\det \mathbf{Z}|$ reflect these geoelectrical contrasts at corresponding skin depths. An example of such distribution can be seen on the map of ρ_{ap_eff} for the period $T = 10$ s (Fig. 4a)—it reveals electrical conductivity heterogeneities at ~3−7 km depths within the sedimentary basin and at larger depths (~7−12 km)—at the edges.

Vector Maps of Geoelectrical Responses to Harmonic Excitation

The impedance data-based vector fields $E(T, x, y)$ of geoelectrical responses to excitation by the E-W or
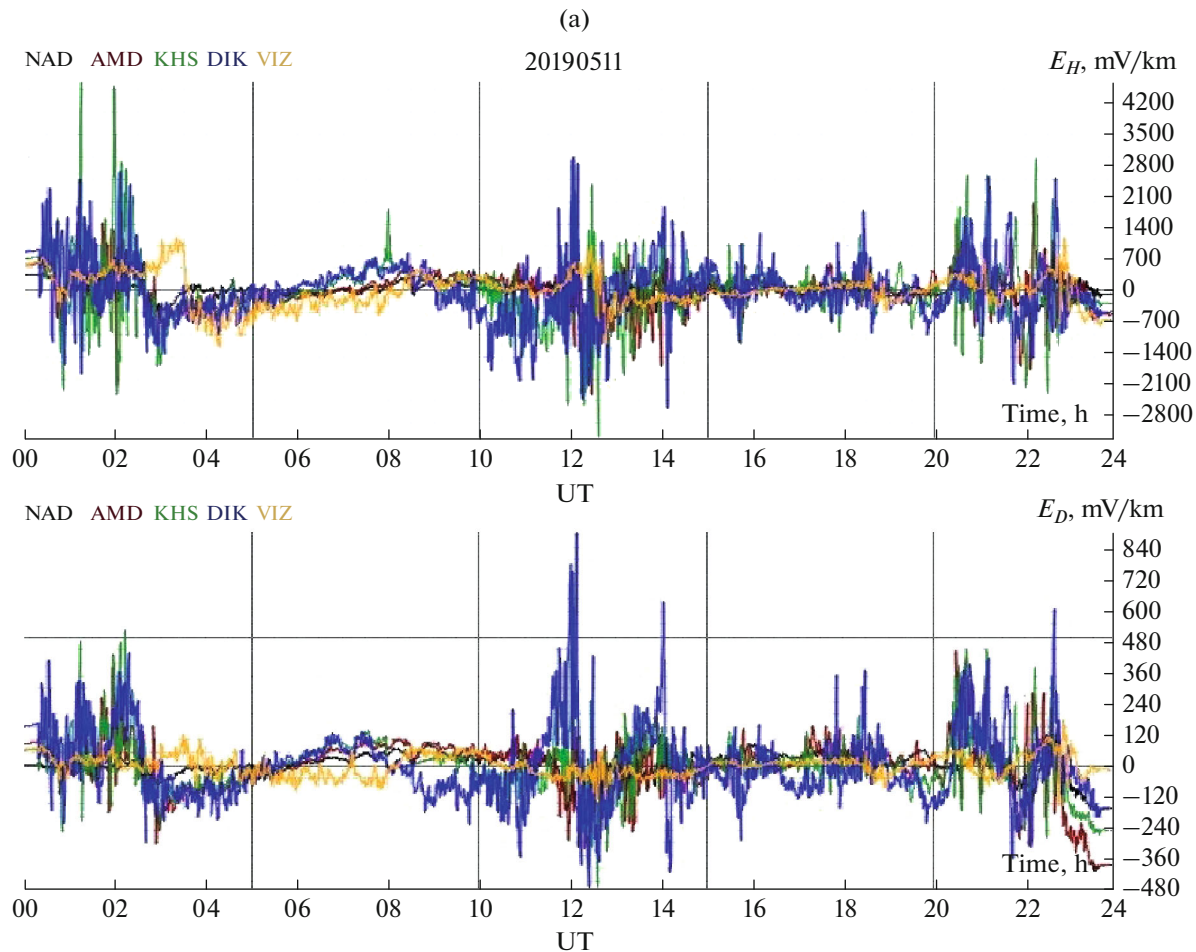
(a)

Fig. 7. Results of synthesis of time series of variations E_H, E_D electric field components by experimental frequency dependences $Z(f)$ at the sounding locations TR10 (a) and NK16 (b) for the record of magnetic variations in the interval 00−24 UT on May 11, 2019 (Fig. 5) at the magnetic observation stations NAD, AMD, KHS, DIK, VIZ. Panel (c) shows time derivatives of variations of the components H and D (nT/s). Locations, frequency dependences $Z(f)$ and the local geoelectrical setting are shown in Fig. 2, Fig. 3, and Fig. 4, respectively.

N-S polarized uniform monochromatic wave $B_h(T)$ with a unit amplitude are shown in Figs. 4b, 4c for $T =$ 10, 100 and 1000 s. The presented estimation periods refer to the ultra-low-frequency (ULF) range of geomagnetic variations, where, according to the available observations and theoretical estimates, GIC amplitudes are the highest (Pilipenko, 2021; Kozyreva et al., 2022).

Thanks to spatial homogeneity of external excitation, these vector distributions can be treated as maps of "geoelectric hazards" for the future YKRT infrastructure: according to the estimated characteristics of telluric fields, we can identify areas of the trough, specific parameters of the geoelectric structure of which show that in these frames, more intense GIC can be expected. Among such areas are the trough edges (points of contact of *MZ* sediments with high-resistivity *PZ* basement), N-W Taimyr area (structures with high electrical conductivity contracts

due to graphite-bearing *PZ* sediment layers), and the YGU area at the trough basement (folded and heterogeneous *PZ* sedimentary formations and magmatic rocks under a thin layer of sediments). To analyze the variability of geoelectrical responses, we selected MT sounding locations in areas with essentially different geoelectric structures (Fig. 2). MT site *NK*16 is located in the area of a deep *MZ* sediment trench and is characterized by distinct one-dimensionality and minimum impedance amplitudes. Locations TR18, TR08 and TR10 are within the YGU with its substantially resistive structure and, at the same time, high-contrast zones characterized by significant variations of MT impedance amplitudes and their exceptional three-dimensionality (Fig. 3, Fig. 4a). At NK16, the geoelectrical response to the individual amplitude magnetic disturbance does not exceed 1−2 mV/km whereas at TR10 the responses are 20 times larger (Figs. 4b, 4c). Throughout the area, maximum amplitudes of the cal-
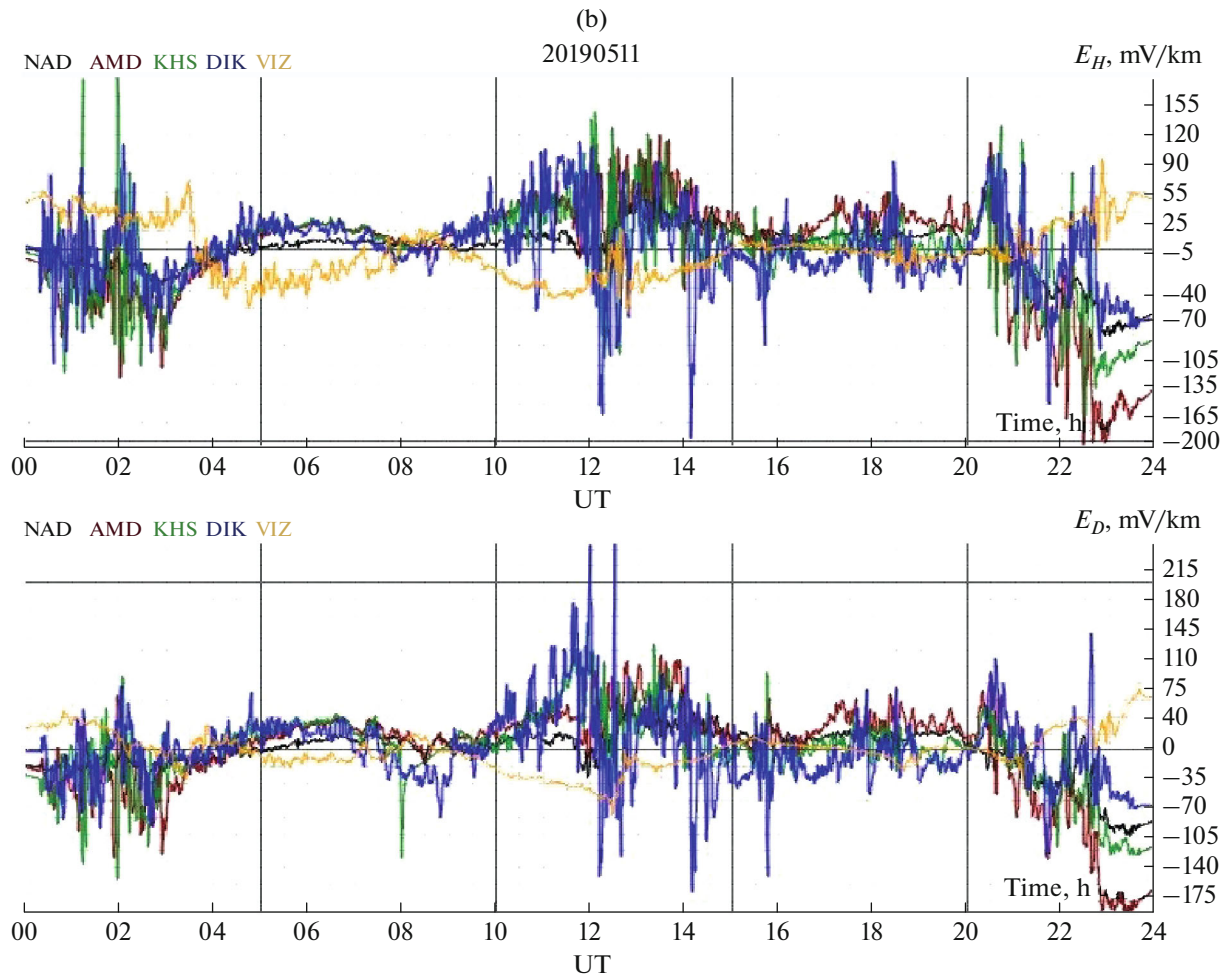
(b)

20190511

Fig. 7. (Contd.).

culated geomagnetically induced electric field also vary tremendously: from units of mV/km in the trough bed to 30 and even 100 mV/km at the edges. The largest are the response amplitudes for the period $T = 10$ s that corresponds to the upper high-resistivity crust, which is recorded for both orthogonal polarizations of the inducing field. Remarkable is the sustaining orientation of the vectors of the strongest responses west of the YGU: perhaps it is due to the linear polarization of the telluric field along extensive N-W Taimyr conductors associated with graphitization.

Comparison of amplitudes of geoelectric fields, synthesized on the basis of the regional set of experimental YKRT impedances (Figs. 4b, 4c), with the results of similar calculations on the basis of model scalar impedances (Kozyreva et al., 2022) is made for the trough region in Figs. 4e, 4f. It demonstrates the general agreement of the amplitude response levels and reveals an expectedly high degree of detail in the pattern of their variability when realistic dense MT observation data are used. Figure 4d shows a fragment of the map of the average electrical conductivity of the

upper 10-km layer of the 3D global model (Alekseev et al., 2015), which was built earlier without regard to the detailed YKRT impedance set. The responses shown in the panels of Figs. 4e, 4f were obtained using scalar, locally normal impedances calculated in this model. The comparison of panels (a) and (d) of Fig. 4 demonstrates the differences in the degree of detail of the idea about the structure of electrical conductivity in the overlap area, and these differences offer opportunities for more sophisticated analysis of variability of the geoelectrical responses calculated on the basis of the experimental MT dataset.

Results of Synthesis of Time Series of Geoelectric Fields for Realistic Geomagnetic Events

Figures 5 and 6 demonstrate three 24-hour records of variations of magnetic field components (in geomagnetic coordinates), from stations in Yamal, Taimyr, and Vize Island. This is a typical example of moderate magnetic storms observed in the central sector of the Arctic, with their substorm components in
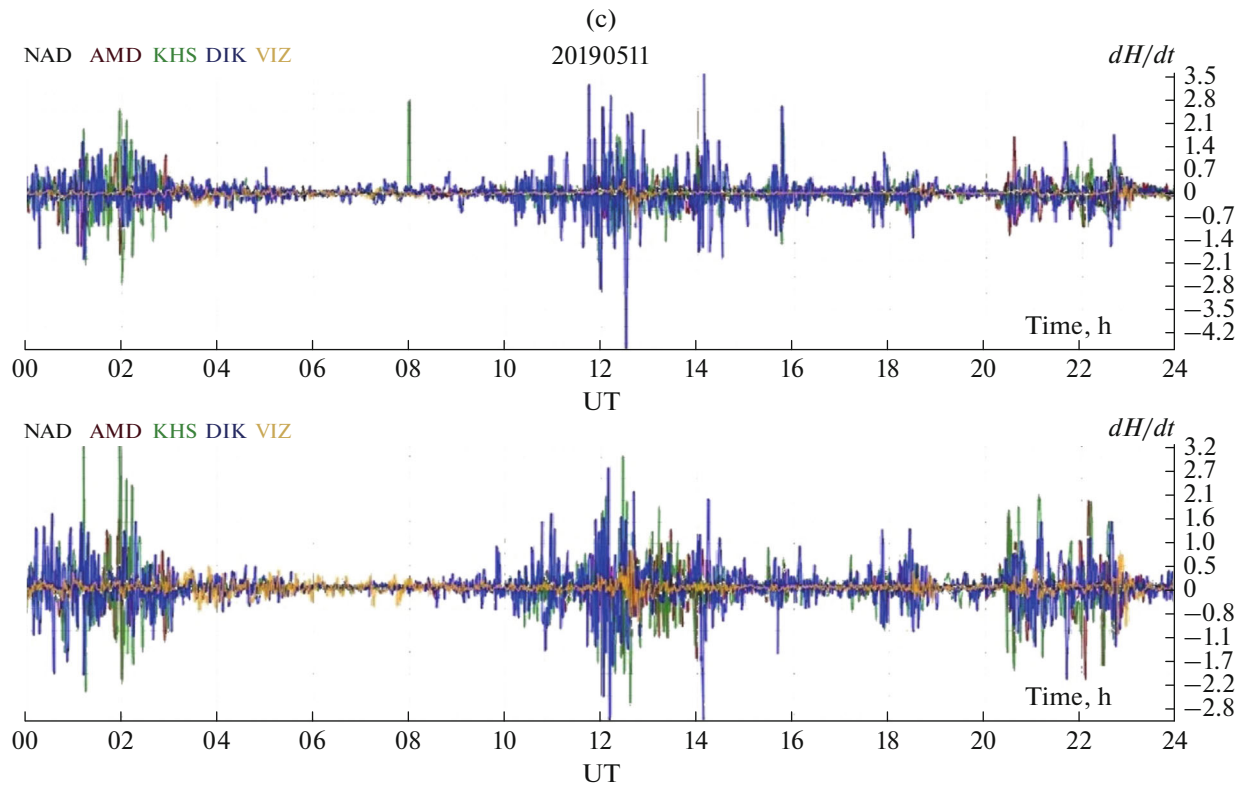
(c)

Fig. 7. (Contd.).

the night-time sector (Fig. 5). Figure 6 presents phenomena that occur more frequently—isolated auroral substorms developing on the average once in three days.

At locations TR10, TR18, TR08, and NK16, geoelectrical responses were synthesized using 24-hour records $\Delta B(t) = \{H(t), D(t)\}$ at the stations VIZ, DIK, AMD, KHS, NAD during a geomagnetic storm on May 11, 2019 (Fig. 7). The first three points are located on the YGU, which is characterized by heterogeneous high-resistivity geoelectrical structure; the last location (NK16) is within a deep sedimentary basin (Fig. 2, Fig. 4a) of the trough. Corresponding impedance tensors differ significantly in amplitudes and frequency dependence patterns (Fig. 3). For calculations, tensors Z were transformed first to geomagnetic coordinates, considering the local magnetic deviation.

It should be noted that the anomalous variations recorded by magnetic stations within the auroral zone (DIK, AMD, KHS) are correlated and fairly close in amplitude levels and amplitude spectra, whereas the variations at the stations outside the auroral oval (VIZ, NAD) differ in their character and are distinctly less intense (Fig. 5—time series, Fig. 8—spectral estimates). As a consequence, similar consistent patterns can be found also in telluric fields synthesized using these five simultaneous magnetic records at different

stations. Synthesis results for the location TR10 are shown in Fig. 7a, for NK16—in Fig. 7b.

For the highly resistive structure at TR10, synthesis using the most variable record at DIK (Fig. 7c) reveals the widest range of responses in E_H—up to 5 V/km during an increase in dB/dt at around 12 UT. At around 2 UT, a local complication of the substorm structure by a series of irregular disturbances is recorded at KHS; presumably, these are characterized by steep edges with high and sign-variable dB/dt. With intense changes in the D-component, the range of the field variations E_H increases to ~7 V/km. At the same time, at NK16 the geoelectrical responses to rapid variations of magnetic fields, damped by thick conductive sedimentary sequence, are no more than 0.4 V/km.

Figure 2 shows vectors of the geomagnetically induced electric fields in 4 locations under analysis, for two moments of the development of a substorm on May 11, 2019, indicated with lines in Fig. 5. This specific example illustrates high temporal and spatial variability of geoelectrical responses, conditioned by changes in external excitation in time as well as by local geoelectric conditions that vary much in space, even at fairly small distances.

Results of another synthesis of geomagnetically induced electric fields' time series are shown in Fig. 9 and Fig. 10. We used the same strongly differing impedance dependences at TR10 and NK16, using
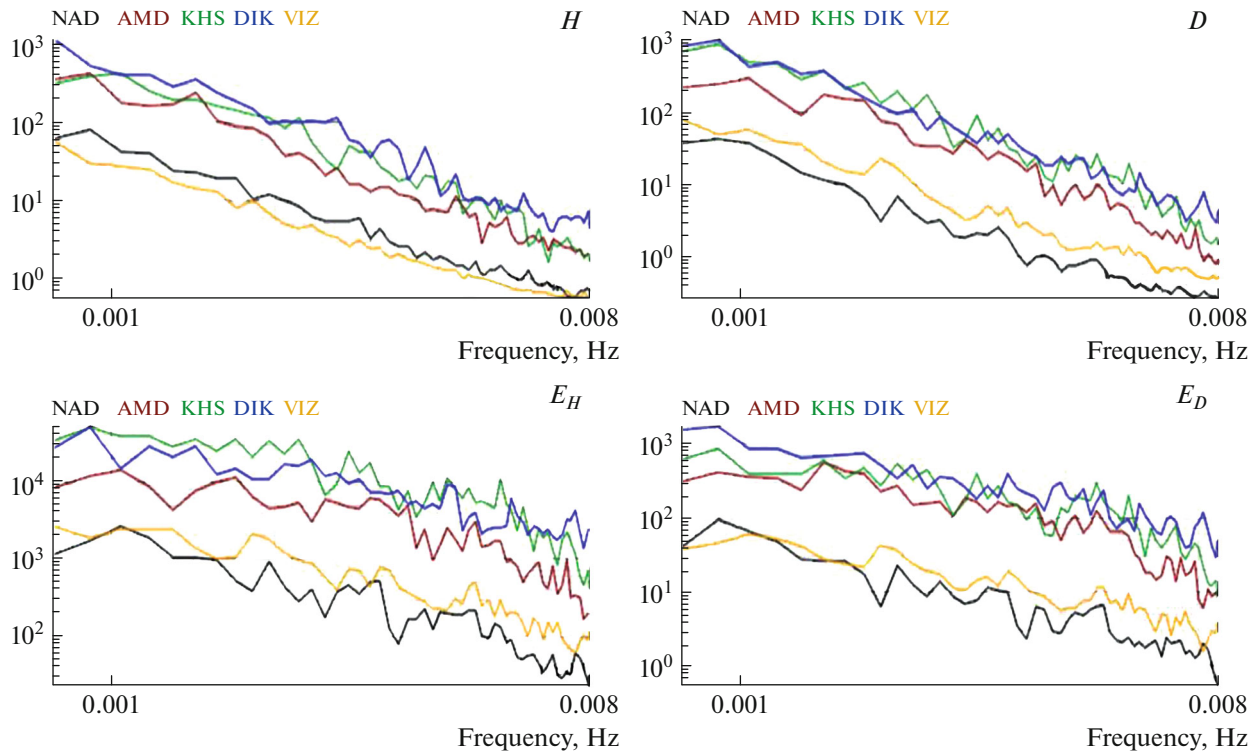
Fig. 8. Frequency dependences of amplitude spectra of magnetic fields ($nT/Hz^{1/2}$), estimated with 128 min window by magnetic records at NAD, AMD, KHS, DIK, VIZ in the time interval 00−24h UT on May 11, 2005, and spectra of corresponding synthesized electric fields ($mW/km \, Hz^{/2}$) for the MT sounding location TR10. Locations are shown in Fig. 2, time series—in Fig. 5.

records of the variations of January 14, 2005 (the fragment from 16 to 24 UT) at CCS, DIC and NOK that are the closest to these locations (Fig. 2). Geomagnetic activity during those hours was due to an intense substorm with the auroral electrojet drifting northward (Fig. 9b). At NOK, the highest amplitude and the earliest origin of a bay-like variation are recorded. At all of the three stations, that variation has quite similar amplitudes and is correlated with time shift. As in the previous example, the maximum rates of changes in the field are observed at DIK, apparently, at the moments the poleward boundary of the northward drifting electrojet is passing over the station.

As shown in Fig. 9a, at TR10 (where the structure is quite resistive for the YKRT) intense dB/dt spikes at ~20:48, ~20:57, and ~23:00 UT correspond to bursts of geoelectrical responses within an amplitude range up to 5 V/km (in E_H) and 2−3 V/km (in E_D). Figure 10a demonstrates the proximity of spectral amplitudes of geomagnetic fields at three stations (with a certain decrease at CCS) and the maintenance of such correlations in the frequency spectra of synthesized telluric fields at TR10 (Fig. 10b). Figure 10c shows amplitude spectra of synthetic fields obtained using the data from the same magnetic stations but for NK16, where the responses to these geomagnetic events are much weaker.

Ways to Improve Derived Estimates

Extending the frequency range of estimates requires additional experimental data. In particular, records of magnetic variations with one-second discretization can help to study, using the available impedance sets, responses in the domain of periods corresponding to the resistive upper-crustal structure of the trough edges and the thick near-surface layer of permafrost. When these objects are excited with sources of the high-frequency segment of the ULF spectrum of geomagnetic events, one would expect larger amplitudes of the telluric field and, consequently, of GIC.

In both approaches used in this paper—the frequency- and the time-domain ones, geoelectrical responses were calculated using the basic assumption that external geomagnetic disturbances are spatially homogeneous. Such an approximation is true when the horizontal disturbance scale exceeds by far the skin depth of the electromagnetic field in the conductive Earth (the White-Price criterion), and is often violated for many realistic sources if one has to deal with large study areas and resistive structures. When obtaining estimates in the frequency domain, this approximation was quite adequate to the formulation of the problem—to build "geoelectric hazards" maps to rank the region according to the relative values of anomalous
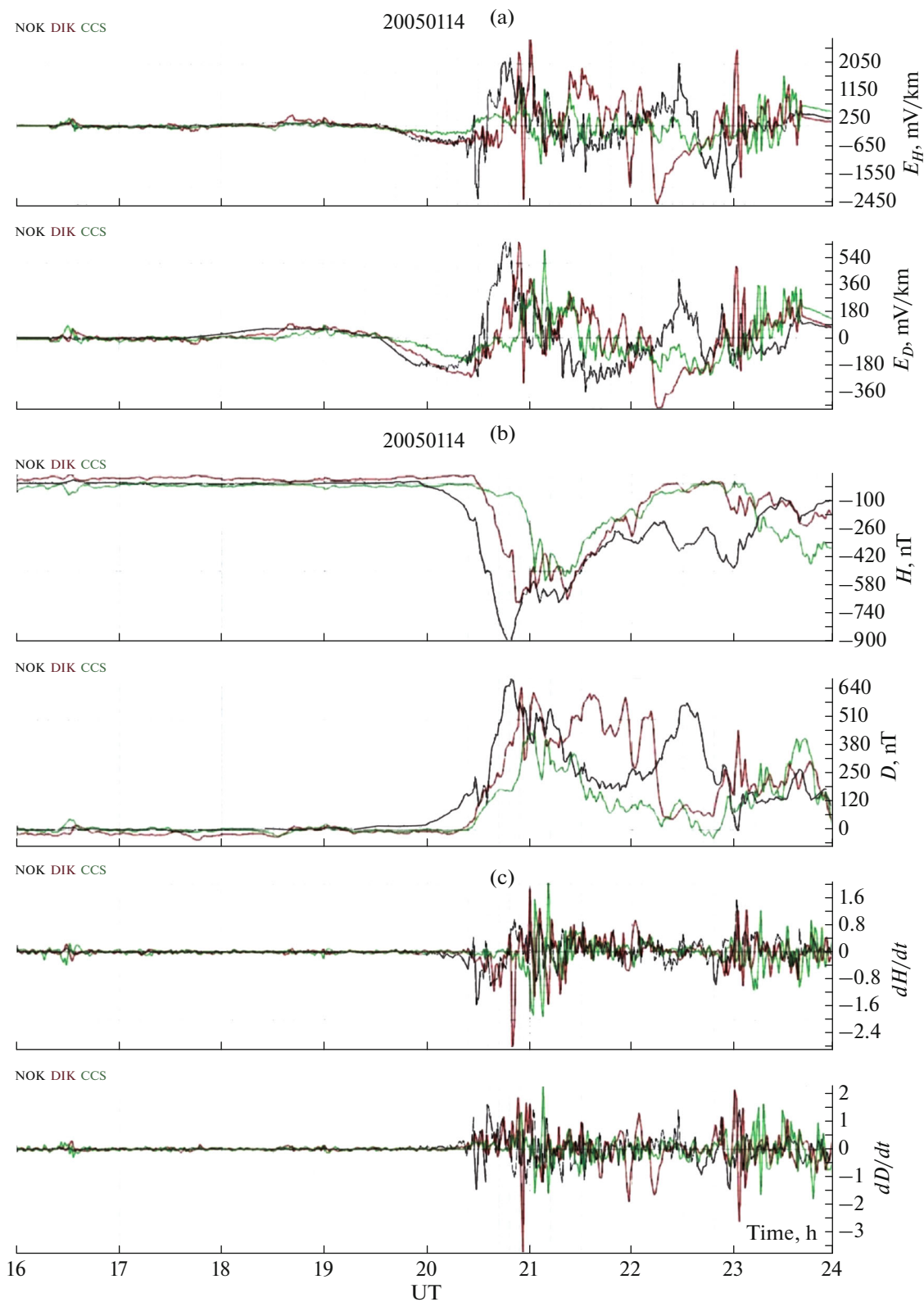
Fig. 9. Results of synthesis of time series of variations E_H, E_D electric field components by experimental estimates of $Z(f)$ at the sounding location TR10 (a) for records of magnetic variations H, D in the interval 16−24 UT on January 1, 2005 (b) at the stationary magnetic observation sites NOK, DIK, CCS. Locations, amplitude frequency dependences of components $Z(f)$ for TR10 and the local geoelectrical setting are shown in Figs. 2−4. Panel (c) shows time derivatives of variations H, D (nT/s).
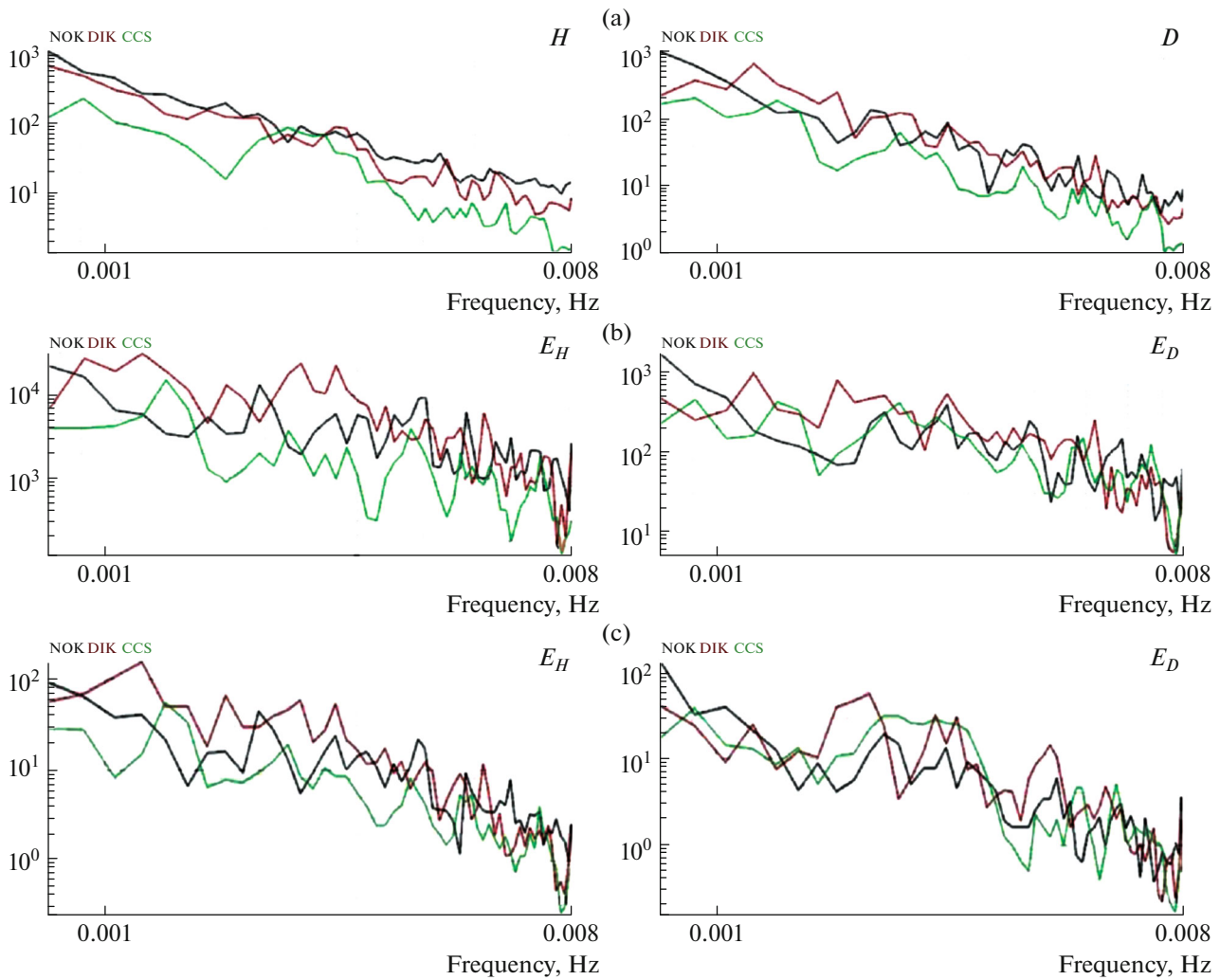
Fig. 10. Frequency dependences of amplitude spectra of magnetic fields (nT/Hz$^{1/2}$), estimated with 128 min window by magnetic records at NOK, DIK, CCS for the time interval 16−24 h UT on January 14, 2005 (a), and spectra of corresponding synthesized electric fields (mW/km Hz$^{1/2}$) for the MT sounding locations TR10 (b) and NK16 (c). Locations are shown in Fig. 2, time series of magnetic fields at these locations and geoelectric fields at TR10 are shown in Fig. 9.

responses of known conductive structures to a certain conditional homogeneous external disturbance (a plane harmonic wave). At the same time, it was assumed that the modern processing methods provide true estimates of MT impedances depending on the geoelectrical structure, and not on the source configuration. The latter is true when the condition of invariability or linear change in space of the horizontal components of the external magnetic source is satisfied (Berdichevsky and Dmitriev, 2009). These conditions can be fulfilled by applying rational criteria for selecting planar events and accumulating adequate amounts of them while processing MT observations made with the use of a remote-reference simultaneous observations (Sokolova and Varentsov, 2007; Pogrebnykh et al., 2022).

In the absence of a dense magnetic observational network, in order to obtain estimates of geoelectrical responses in the time domain we used events recorded by magnetic stations located at a distance from the MT sounding site. This approach is pragmatically followed in numerous GIC studies, for example, in (Dimmock et al., 2019) and others. Above, we pointed out the correlation of the geomagnetic disturbances recorded at the stations of the auroral zone, certain proximity of their amplitudes (Fig. 5—a magnetic storm; Figs. 6a, 6b—substorms, north- and southward drifting of auroral electrojets, respectively), and their quite closely grouped amplitude spectra that are much larger than the spectra of the variations at VIZ and NAD located at a distance from that zone (Fig. 8, Fig. 10). This makes it possible to view as credible the estimates derived by the local impedances and records at a station closest to the YKRT (NOK or DIK), as rational "proxies" of extreme geoelectrical responses in the targeted characteristic areas of the trough.

A more detailed spatial pattern of the distribution of geoelectrical responses can be reconstructed on the basis of estimates (using the available field MT observations of the YKRT) of horizontal magnetic tensors that link magnetic fields at local sounding sites with their synchronous analogues at sites closest to magnetic stations. A similar approach was used in (Campanyà et al., 2019), whereas interpolation of magnetic station network data for updating the spatial external excitation model—in (Dimmock et al., 2019; Bedrosian and Love, 2015). The labour-intensive task to build a system of horizontal magnetic field tensors for the YKRT territory was partially completed during prospecting sounding works of Nord West Ltd in the S-E section of the trough extremity (Pogrebnykh et al., 2022). The results showed that changes in the ULF range of magnetic field can exceed 5−7% in the absolute value and 3° in phase already at a distance of more than 10 km.

Hazards to the Regional YKRT Infrastructure from Space Weather Disturbances

The only infrastructure facility operated in the YKRT area since 1969 to the present is the Messoyakha-Norilsk gas pipeline. This world's first gas pipeline beyond the Arctic Circle links the Messoyakha gas condensate field and the Norilsk Mining and Smelting Works, running under Yenisei and crossing 86 rivers, 15 large lakes and swamps (Fig. 2). Along most of its 263 km length, the pipeline rests on steel supports, and has advanced anti-corrosion coating and cathodic protection. In the conditions of marshy tundra, continuous and island permafrost, even minor damages to the coating will cause fast progressing of defects and severe electrochemical corrosion. The cumulative effect of recurring excesses of cathodic protection level due to variations in the pipe-to-soil potential during geomagnetic disturbances and GIC flowing significantly increases corrosion. For instance, long-lasting activity of quasi-periodic geomagnetic pulsations sometimes poses a greater hazard than short-term GIC spikes during an explosive substorm commencement. Peaks in the periods inherent in Pi3 pulsations (3, 4, 10 min) can be found in the spectral features of the analyzed auroral substorms (Fig. 8, Fig. 10). Close to near east-west, regional MT field polarization in the ULF range, determined by the strike of conductive sedimentary formations of the trough (Slinchuk et al., 2022; Yakovlev et al., 2021), amplifies induced currents in the grounded metal structures of the gas pipeline, also trending east-west.

In order to take GIC estimates into account when designing and optimizing measures of protection against destructive effects of space weather, these estimates can be obtained based on the geoelectrical responses to typical geomagnetic disturbances and technical parameters of infrastructure sites. In case of the Messoyakha-Norilsk gas pipeline, this process requires an in-depth analysis of NOK magnetic records in order to gather statistics on the recorded anomalous geomagnetic disturbances, as well as the utilization of the data obtained with the use of the existing and, if possible, additional MT soundings in the vicinity of the gas pipeline. Similar prior estimates can be derived also for "virtual" lines of the YKRT future infrastructure facilities.

CONCLUSIONS

The conducted study laid the foundation for the required prediction of risks associated with the effect of space weather anomalies on the existing and future technological infrastructure in the Yenisei-Khatanga regional trough, a vast high-potential oil and gas area in the central sector of the Russian Arctic. It has been demonstrated that for an adequate assessment of these risks it is necessary to carefully analyze the geoelectric structure of the area/region of interest, since heterogeneities in the distribution of electrical conductivity of the Earth's crust can be a major factor for the GIC patterns, by damping or, on the contrary, significantly amplifying current amplitudes and modulating the spectral composition.

As a result of the comparison of the constructed maps of the synthesized telluric field components' distribution to the geologic data, we have identified the target region's geological structural areas characterized by the most intense responses. The estimates of vectors of the horizontal geoelectric field E, induced by the harmonic oscillations $B_h(T)$, vary greatly in magnitude and direction. At frequencies that carry most of the disturbed field's energy, they have the maximum amplitudes in the range from <1 to ~50−100 mV/km at a unit amplitude of external magnetic field variations. The strongest are the geoelectrical responses of Paleozoic resistive formations that are exposed in the trough edges or close to the surface (Yangodo-Gorbitsky Uplift). Due to the revealed hydrocarbon potential (Afanasenkov et al., 2018), these formations appear more and more interesting for petroleum experts. It is possible, indeed, that developing an infrastructure in their area can become a priority relatively soon. Even with moderate amplitudes of geomagnetic variations during substorms (300−500 nT), their geoelectrical responses in such setting can reach more than 15 V/km, thus, seriously threatening cathodic protection of future gas pipelines. It has been shown that during a mild magnetic storm on May 11, 2019 with Dst ~−60 nT and a substorm on January 14, 2005, telluric field variations for several geoelectrical structures of the YKRT (specifically, on the YGU of the folded basement of the trough) might have exceeded 5−7 V/km.

In the design of the regional infrastructure (pipelines, future ETLs), the obtained estimates of possible amplitudes and directions of the geoelectric field, supplemented by the information on the geometry and

electrical parameters of designed facilities, can be used for the calculation of extreme GIC for the optimization of the proposed variants of the protection systems (cathodic protection of pipelines, electronic monitoring systems, etc.) from possible destructive effects of violent geomagnetic disturbances.

CONFLICT OF INTEREST

The authors declare that they have no conflicts of interest.

REFERENCES

Afanasenkov, A.P. and Yakovlev, D.V., Application of electrical prospecting methods to petroleum exploration on the northern margin of the Siberian Platform, *Russ. Geol. Geophys.*, 2018, vol. 59, no. 7, pp. 827−845.

Afanasenkov, A.P., Obukhov, A.N., Bondarenko, M.T., Bordyug, A.V., Dakhnova, M.V., Ermolova, T.E., Kirsanov, A.M., Kondratiev, I.K., Kopilevich, E.A., Korneev, A.A., Kravchenko, M.N., Kucherya, M.S., Levchuk, L.V., Lybaev, R.R., Mushin, I.A., et al., Methodology of comprehensive geological and geophysical studies of underinvestigated oil and gas-bearing areas of the Russian Federation: the case of the northern margin of the Siberian Platform, in *VNIGNI − 65: Lyudi, rezul'taty i perspektivy* (VNIGNI—65: People, Results and Prospects), Varlamov, A.I. and Petersilye, V.I., Eds., Moscow: VNIGNI, 2018, pp. 150−210.

Alekseev, D., Kuvshinov, A., and Palshin, N., Compilation of 3D-global conductivity model of the Earth for space weather applications, *Earth, Planets Space*, 2015, vol. 67, Article ID 108.
https://doi.org/10.1186/s40623-015-0272-5

Andreev, V.S., Biserkin, I.A., Bol'shakov, E.M., Dovydenko, G.M., Pimanova, N.N., Sokolova, E.Yu., Spiridonov, V.A., and Shpektrov, A.L., Morphostructural and physical characteristics of magmatic formations within Yenisei-Khatanga Trough: new results of geophysical data analysis, *Geol. Nefti Gaza*, 2021, no. 6, pp. 83−105.
https://doi.org/10.31087/0016-7894-2021-6-83-105

Apatenkov S.V., Pilipenko V.A., Gordeev E.I., Viljanen, A., Juusola, L., Belakhovsky, V.B., Sakharov, Ya.A., and Se-livanov, V.N., Auroral omega bands are a significant cause of large geomagnetically induced currents, *Geophys. Res. Lett.*, 2020, vol. 47, no. 6, Article ID e2019GL086677.
https://doi.org/10.1029/2019GL086677

Bedrosian, P.A. and Love, J.J., Mapping geoelectric fields during magnetic storms: Synthetic analysis of empirical United States impedances, *Geophys. Res. Lett.*, 2015, vol. 42, no. 23, pp. pp. 10160−10170.
https://doi.org/10.1002/2015GL066636

Belakhovsky, V.B., Pilipenko, V.A., Sakharov, Ya.A., and Selivanov, V.N., Characteristics of the variability of a geomagnetic field for studying the impact of the magnetic storms and substorms on electrical energy system, *Izv., Phys.Solid Earth*, 2018, no. 1, pp. 52−65.

Berdichevsky, M.N. and Dmitriev, V.I., *Modeli i metody magnitotelluriki* (Models and Methods of Magnetotellurics), Moscow: Nauchnuy Mir, 2009.

Boteler, D.H., Pirjola, R.J., and Nevanlinna, H., The effects of geomagnetic disturbances on electrical systems at the Earth's surface, *Adv. Space Res.,* 1998, vol. 22, no. 1, pp. 17−27.

Brasse, H. and Junge, A., The influence of geomagnetic variations on pipelines and an application for large-scale magnetotelluric depth sounding, *J. Geophys.,* 1984, vol. 55, pp. 31−36.

Campbell, W.H., Induction of auroral zone electric currents within Alaska pipeline, *Pure Appl. Geophys.,* 1978, vol. 116, no. 6, pp. 1143−1173.

Campanyà, J., Gallagher, P.T., Blake, S.P., Gibbs, M., Jackson, D., Beggan, C.D., Richardson, G.S., and Hogg. C., Modelling geoelectric fields in Ireland and the UK for space weather applications, *Space Weather*, 2019, vol. 17, pp. 216−237.
https://doi.org/10.1029/2018SW001999

Cannon, P., Barclay, L., Curry, C., Dyer, C., Edwads, R., Greene, G., Hapgood, M., Horne, R.B., Jackson, D., Mitchell, C.N., Owen, J., Richards, A., Rogers, C., Ryden, K., Saunders, S., Sweeting, M., Tanner, R., Thomson, A., and Underwood, C., *Extreme Space Weather: Impacts on Engineered Systems and Infrastructure*, London: Royal Acad. Eng., 2013.

Chinkin, V.E., Soloviev, A.A., Pilipenko, V.A., Engebretson, M.J., and Sakharov, Ya.A., Determination of vortex current structure in the high-latitude ionosphere with associated GIC bursts from ground magnetic data, *J. Atmos. Sol.-Terr. Phys.*, 2021, vol. 212, Article ID 105514.
https://doi.org/10.1016/j.jastp.2020.105514

Cordell, D., Unsworth, M.J., Lee, B., Hanneson, C., Milling, D.K., and Mann, I.R., Estimating the geoelectric field and electric power transmission line voltage during a geomagnetic storm in Alberta, Canada using measured magnetotelluric impedance data: The influence of three-dimensional electrical structures in the lithosphere, *Space Weather*, 2021, vol. 19, no. 10, Article ID e2021SW002803.
https://doi.org/10.1029/2021SW002803

Evaluation of possible corrosion enhancement due to telluric currents: case study of Bolivia-Brazil pipeline, *Ann. Geophys.,* 2020, vol. 38, pp. 881−888.

Dimmock A.P., Rosenqvist L., Hall J.-O., Viljanen A., Yordanova E., Honkonen I., André, M., and Sjöberg, E.C., The GIC and geomagnetic response over Fennoscandia to the 7−8 September 2017 geomagnetic storm, *Space Weather*, 2019, vol. 17, no. 7, pp. 989−1010. https://doi.org/10.1029/2018SW002132

Dimmock, A.P., Rosenqvist, L., Welling, D.T., Viljanen, A., Honkonen, I., Boynton, R.J., and Yordanova, E., On the regional variability of dB/dt and its significance to GIC, *Space Weather*, 2020, vol. 18, no.8, Article ID e2020SW002497. https://doi.org/10.1029/2020SW002497

Epishkin, D.V., Improving magnetotelluric data processing methods, *Moscow Univ. Geol. Bull.,* 2016, vol. 71, no. 5. pp. 347−354.

Ernst, T., Sokolova, E.Yu., Varentsov, I.M., and Golubev, N.G., Comparison of two MT data processing techniques using synthetic data sets, *Acta Geophys. Pol.,* 2001, vol. 49, no. 2, pp. 213−244.

Gvishiani, A.D. and Lukianova, R.Yu., Geoinformatics and observations of the Earth's magnetic field: The Russian segment, *Izv., Phys.Solid Earth*, 2015, vol. 51, no. 2, pp. 157−175.

Ivannikova, E., Kruglyakov, M., Kuvshinov, A., Rastätter, L., Pulkkinen, A., Regional 3-D modeling of ground electromagnetic field due to realistic geomagnetic disturbances, *Space Weather*, 2018, vol. 16, no. 5, pp. 476−500. https://doi.org/10.1002/2017SW001793

Kelbert, A., The role of global/regional earth conductivity models in natural geomagnetic hazard mitigation, *Surv. Geophys.*, 2020, vol. 41, no. 1, pp. 115−166. https://doi.org/10.1007/s10712-019-09579-z

Kelbert, A., Meqbel, N., Egbert, G.D., and Tandon, K., ModEM: A modular system for inversion of electromagnetic geophysical data, *Comput.Geosci.,* 2014, vol. 66, pp. 40−53.

Kleymenova, N.G. and Kozyreva, O.V., Magnetic storms and heart attacks: Are storms always dangerous?, *Geofiz. Prots. Biosf.*, 2008, vol. 7, no. 3, pp. 5−24.

Kozyreva, O., Pilipenko, V., Sokolova, E., Sakharov, Ya., and Epishkin, D., Geomagnetic and telluric field variability as a driver of geomagnetically induced currents, in *Problems of Geocosmos-2018: Springer Proc. in Earth and Environ. Sci.,* Yanovskaya, T., Kosterov, A., Bobrov, N., Divin, A., Saraev, A., and Zolotova, N., Eds., Cham: Springer, 2019, pp. 297−307. https://doi.org/10.1007/978-3-030-21788-4_26

Kozyreva, O., Pilipenko, V., Krasnoperov, R., Baddeley, L., Sakharov, Ya., and Dobrovolsky, M., Fine structure of substorm and geomagnetically induced currents, *Ann. Geophys.*, 2020, vol. 63, no.2, Article ID GM219. https://doi.org/10.4401/ag-8198

Kozyreva, O.V., Pilipenko, V.A., Marshalko, E.E., Sokolova, E.Yu., and Dobrovolsky, M.N., Monitoring of Geomagnetic and Telluric Field Disturbances in the Russian Arctic, *Appl. Sci.,* 2022, vol. 12, Article ID 3755. https://doi.org/10.3390/app12083755

Love, J.J., Pulkkinen, A., Bedrosian, P.A., Jonas, S., Kelbert, A., Rigler, E.J., Finn, C.A., Balch, C.C., Rutledge, R., Waggel, R.M., Sabata, A.T., Kozyra, J.U., and Black, C.E., Geoelectric hazard maps for the continental United States, *Geophys. Res. Lett.*, 2016, vol. 43, no. 18, pp. 9415−9424. https://doi.org/10.1002/2016GL070469

Lucas, G.M., Love, J.J., and Kelbert, A., Calculation of voltages in electric power transmission lines during historic geomagnetic storms: An investigation using realistic earth impedances, *Space Weather*, 2018, vol. 16, no. 2, pp. 185−195. https://doi.org/10.1002/2017SW001779

Marshalko, E., Kruglyakov, M., Kuvshinov, A., Juusola, L., Kwagala, N.K., Sokolova, E., and Pilipenko, V., Comparing three approaches to the inducing source setting for the ground electromagnetic modeling due to space weather events, *Space Weather*, 2021, vol. 19, no. 2, Article ID e2020SW002657. https://doi.org/10.1029/2020SW002657

Osella, A., Favetto, A., and López, E., Currents induced by geomagnetic storms on buried pipelines as a cause of corrosion, *J. Appl. Geophys.*, 1998, vol. 38, no. 3, pp. 219−233.

Pilipenko, V.A., Space weather impact on ground-based technological systems, *Sol.-Terr. Phys.*, 2021, vol. 7, no. 3, pp. 68−104. https://doi.org/10.12737/stp-73202106

Pilipenko, V.A., Vellante, M., Anisimov, S., De Lauretis, M., Fedorov, E.N., and Villante, U., Multi-component ground-based observation of ULF waves: goals and methods, *Ann. Geofis.*, 1998, vol. 41, no. 1, pp. 63−77.

Pirjola, R., Kauristie, K., Lappalainen, H., Viljanen, A., and Pulkkinen, A., Space weather risk, *Space Weather*, 2005, vol. 3, Article ID S02A02.

Pogrebnykh, E.O., Yakovlev, D.V., Epishkin, D.V., and Yakovlev, A.G., The validity of using a plane wave model and duel-channel measurement systems in MT sounding in polar latitudes, *Izv., Phys. Solid Earth*, 2022, no. 5. In press.

Pulkkinen, A., Pirjola, R., Boteler, D., Viljanen, A., and Yegorov, I., Modelling of space weather effects on pipelines, *J. Appl. Geophys.*, 2001, vol. 48, no. 4, pp. 233−256. https://doi.org/10.1016/S0926-9851(01)00109-4

Pulkkinen, A., Bernabeu, E., Thomson, A., Viljanen, A., Pirjola, R., Boteler D., Eichner, J., Cilliers, P.J., Welling, D., Savani, N.P., Weigel, R.S., Love, J., Balch, Ch., Ngwira, C.M., Crowley, G., Schultz, A., Kataoka, R., Anderson, B., Fugate, D., Simpson, J.J., and MacAlester, M., Geomagnetically induced currents: Science, engineering and applications readiness, *Space Weather*, 2017, vol. 15, no. 7, pp. 828−856. https://doi.org/10.1002/2016SW001501

Püthe, C. and Kuvshinov, A., Towards quantitative assessment of the hazard from space weather: Global 3D-modellings of the electric field induced by a realistic geomagnetic storm, *Earth, Planets Space*, 2013, vol. 65, no. 9, pp. 1017−1025.

Sakharov, Ya.A., Yagova, N.V., and Pilipenko, V.A., Pc5/Pi3 geomagnetic pulsations and geomagnetically induced currents, *Bull. Russ. Acad. Sci.: Phys.*, 2021, vol. 85, no. 3, pp. 329−333. https://doi.org/10.3103/S1062873821030217

Slinchuk, G.E., Yakovlev, D.V., Yakovlev, A.G., Andreev, M.A., and Shirokova, Ye.P., A depth three-dimen-

sional geoelectrical model of Taimyr, *Izv.*, *Phys. Solid Earth*, 2022, no. 5. In press.

Sokolova, E.Yu., Varentsov, Iv.M., and BEAR Collab., Deep array electromagnetic sounding on the Baltic Shield: external excitation model and implications for upper mantle conductivity studies, *Tectonophysics*, 2007, vol. 445, nos. 1—2, pp. 3—25.

Sokolova, E.Yu., Kozyreva, O.V., Pilipenko, V.A., Sakharov, Ya.A., and Epishkin, D.V., Space-Weather-Driven Geomagnetic- and Telluric-Field Variability in Northwestern Russia in Correlation with Geoelectrical Structure and Currents Induced in Electric-Power Grids,

Izv., Atmos. Ocean. Phys., 2019, vol. 55, no. 11, pp. 1639—1658. https://doi.org/10.1134/S000143381911015X

Trichtchenko, L. and Boteler, D.H., Modelling of geomagnetic induction in pipelines, *Ann. Geophys.,* 2002, vol. 20, no. 7, pp. 1063—1072. https://doi.org/10.5194/angeo-20-1063-2002

Vakhnina, V.V., *Modelirovaniye rezhimov raboty silovykh transformatorov system elektrosnabzheniya pri geomagnitnykh byryakh* (Modeling Operation Modes of Power Transformers of Electric Power Grids during Geomagnetic Storms), Tolyatti: TGU, 2012.